Eur. Phys. J. B **13**, 157–168 (2000)

THE EUROPEAN PHYSICAL JOURNAL B

EDP Sciences

Lateral current density fronts in globally coupled bistable semiconductors with S- or Z-shaped current voltage characteristics

M. Meixner[1], P. Rodin[2], E. Schöll[1,a], and A. Wacker[1]

[1] Institut für Theoretische Physik, Technische Universität Berlin, Hardenbergstrasse 36, 10623, Berlin, Germany
[2] Ioffe Physicotechnical Institute of Russian Academy of Sciences, Politechnicheskaya 26, 194021, St. Petersburg, Russia

Received 19 March 1999

Abstract. We study the propagation of a lateral current density front in a bistable semiconductor system with S- or Z-shaped current-voltage characteristics. It is demonstrated that an external load circuit introduces a global coupling which leads to positive or negative feedback upon the front dynamics in S- or Z-type systems, respectively. This results in accelerated or decelerated front motion. The type of feedback can be reversed if the system is operated in an active external circuit with negative load resistance. Double barrier resonant tunneling diodes (DBRT) and heterostructure hot electron diodes (HHED) are used as examples of Z- and S-type systems, respectively.

PACS. 05.70.Ln Nonequilibrium and irreversible thermodynamics – 72.20.Ht High-field and nonlinear effects – 85.30.-z Semiconductor devices

1 Introduction

Travelling front patterns in bistable and excitable active media [1] represent a universal phenomenon which occurs in nonlinear spatially extended systems of different nature, ranging from physics [2–7] and chemistry [8] to biology and ecology [9,10]. In many cases in addition to a local diffusive coupling such systems also experience a *global coupling*. Generally, global coupling is related to external constraints imposed upon the system's dynamics. In the presence of global coupling, some dynamic variables of the active media (*e.g.*, the global excitation level) depend on the spatially averaged parameters of the travelling pattern. Recently, global coupling has been widely recognized as an important factor for spatio-temporal dynamics in spatially extended systems. It has been studied in different models, *e.g.*, Landau-Ginzburg amplitude equations [11,12], arrays of discrete oscillators [13], reaction-diffusion systems [14–18], surface reactions [19,20] and electro-chemical systems [21].

In *bistable semiconductor systems* the global coupling represents an inherent feature of spatio-temporal dynamics of the current density patterns (*e.g.*, current filaments [22], fronts and pulses [23]). The mechanism of this coupling is as follows. For any evolution of the current density pattern which is accompanied by the variation of the total current through the device, the voltage drop at an external load and/or internal series resistance changes. That causes a variation of the voltage u dropping across the device which usually characterizes the global excitation level of the bistable semiconductor system. This type of feedback is well-known with respect to stationary [22,24–26] and spiking [27,28] current filaments.

In this article we study the effect of global coupling on the propagation of *lateral current density fronts*. Excitation of such fronts, propagating in the direction perpendicular to the direction of the current flow, is possible for systems with bistable current-voltage characteristics if the low current state and the high current state coexist in a certain interval of the voltage u. Such bistability may be associated either with an S- or a Z-shaped current density *versus* voltage characteristic (Fig. 1) [29]. An S-shaped characteristic represents a classical example of bistability in both bulk semiconductors (*e.g.*, due to an overheating instability [24] or impact ionization breakdown [22]) and layered semiconductor structures (in *p-i-n*-diodes [30], avalanche transistors [31], heterostructure hot-electron diodes (HHED) [27,32,33], *p-n-p-n*- [34] and *p-n-p-i-n*-multilayered structures [35,36]). The S-shaped characteristic also includes the whole family of switching devices of modern electronics (thyristors, MOSFET, etc.) [37]. The *Z-shaped bistability* has only recently received attention; it occurs, *e.g.*, in double barrier resonant tunneling structures (DBRT) [38] and gate-driven *p-n-p-n*-structures [39]. Transverse current density fronts in DBRT have recently been discussed in [40,41]. S- and Z-type systems constitute the major classes of bistable semiconductors. The aim of this article is to reveal similarities and differences between globally coupled dynamics of lateral

[a] e-mail: schoell@physik.tu-berlin.de

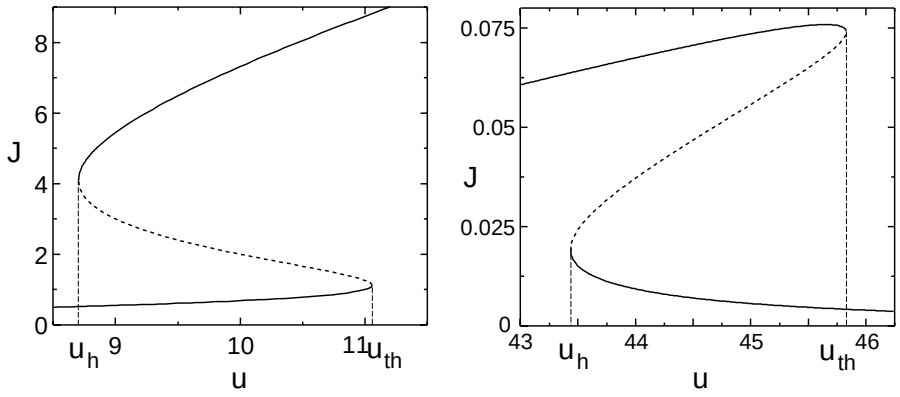

Fig. 1. (a) S-shaped and (b) Z-shaped current-voltage characteristics $J(u)$. The threshold voltage $u_{\rm th}$ and the holding voltage $u_{\rm h}$ mark the boundaries of the bistability domain. The characteristics are calculated (a) for the heterostructure hot electron diode (HHED) (see Eq. (6), $T = 0.05$) and (b) for the double barrier resonant tunneling structure (DBRT) (see Eq. (7), the numerical parameters are given in the Appendix).

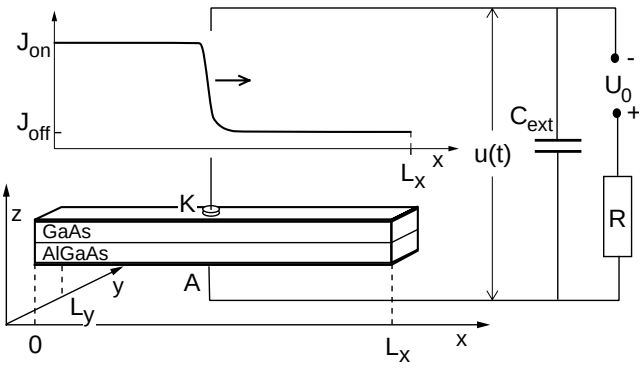

Fig. 2. Sketch of the bistable semiconductor element and the external circuit (bias U_0, load resistor R, capacitor $C_{\rm ext}$). The GaAs/AlGaAs heterostructure hot electron diode (HHED) is shown as an example. The cathode (K) and anode (A) contacts are equipotential surfaces, and therefore the voltage $u(t)$ across the device is independent of x and y. An inhomogeneous current density distribution $J(x)$ corresponding to a front propagating in lateral x-direction is shown as an inset.

current density patterns for these two classes of bistable systems and illustrate these findings with two significant examples, *viz.* the HHED and the DBRT.

We consider one-dimensional fronts propagating along the x-axis in long, narrow samples as sketched in Figure 2, where the second transverse dimension L_y (along the y-axis) is so short that pattern formation cannot develop. For a wide class of semiconductor systems the internal state can be characterized by a single variable $a(x,t)$ which corresponds to the internal degree of freedom relevant for the bistability. The physical meaning of the variable a might be a concentration of excess carriers [22], electron temperature [24,25], interface charge density [27], or the electric potential drop across one of the *pn* junctions [31,34], depending upon the specific transport mechanism. The reduced dynamical description in terms of this variable can be derived from a full 3D transport model, the Poisson equation and continuity equations *via* adiabatic elimination of fast variables as done, for instance, in [24,27,31,34,35,40,41] for various semiconductor systems. This equation takes the form of a reaction-diffusion equation

$$\tau_a \frac{\partial a(x,t)}{\partial t} = l^2(a) \frac{\partial^2 a(x,t)}{\partial x^2} + f(a(x,t), u(t)). \qquad (1)$$

Here τ_a and l are the relaxation time and diffusion length of the variable a, respectively. Generally, the combination of lateral diffusion and drift (due to the lateral electrical field induced by an inhomogeneous charge distribution) effectively results in a term with a-dependent diffusion coefficient $D(a) \equiv l^2(a)/\tau_a$ [29,40–42] (see also Appendix). Here for simplicity we set $l = \text{const}$. We assume passive boundaries described by Neumann boundary conditions for $a(x,t)$

$$\frac{\partial a(0,t)}{\partial x} = \frac{\partial a(L_x,t)}{\partial x} = 0. \qquad (2)$$

The temporal dynamics of the voltage $u(t)$ across the device is described by Kirchhoff's equation for the external circuit:

$$\tau_u \frac{{\rm d}u}{{\rm d}t} = U_0 - u(t) - RL_y \int_0^{L_x} J(a,u){\rm d}x,$$
$$\tau_u \equiv RC, \quad C \equiv C_{\rm ext} + C_{\rm int}, \qquad (3)$$

where $J(a,u)$ is the current density in a cross-section of the system, which is determined locally by the internal variable a and the voltage drop u, U_0 is the applied bias voltage, R is the load resistance, $C_{\rm int}$ is the internal differential capacitance of the sample, $C_{\rm ext}$ is the capacitance in the external circuit (see Fig. 2). Equation (3) describes the *global constraint* imposed upon the internal dynamics of the current density pattern by the external circuit.

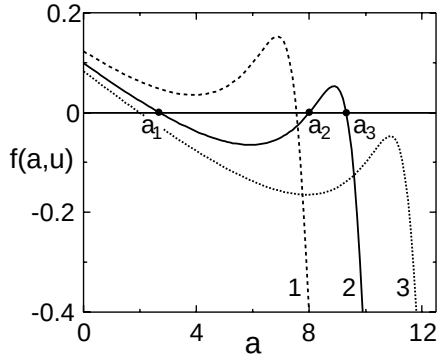

Fig. 3. The local kinetic function $f(a,u)$ as a function of the internal variable a for $u < u_{\rm h}$ (curve 1), $u_{\rm h} < u < u_{\rm th}$ (curve 2), and $u > u_{\rm th}$ (curve 3). The model of the heterostructure hot electron diode (see Eq. (6)) where large a corresponds to small values of the current density J is used as numerical example ($T = 0.05$).

Note that in contrast to the case considered in [14,18,25, 43] this constraint has the form of a *dynamical* equation for the global excitation parameter u.

The local kinetic function $f(a,u)$ is a non-monotonic function of a which for $u_{\rm h} < u < u_{\rm th}$ has three zeros $a_1 < a_2 < a_3$ reflecting the bistability (Fig. 3). For the homogenous steady state, the local dependence $a(u)$ is calculated from the null-isocline $f(a,u) = 0$ and inserted into $J(a,u)$ in order to determine the local current density as a function of the voltage $j(u) \equiv J(a(u),u)$. Here we restrict ourselves to the case where the resulting current-voltage characteristic is S- or Z-shaped. We denote the current density in the high conductivity and low conductivity states by $J_{\rm on}$ and $J_{\rm off}$, respectively. The value a_2 corresponds to the state on the intermediate branch of the current-voltage characteristic. The higher value of a does not necessarily correspond to the higher value of the current density J and both situations ($a_1 \to J_{\rm off}, a_3 \to J_{\rm on}$) and ($a_1 \to J_{\rm on}, a_3 \to J_{\rm off}$) are possible in different systems.

In the following we assume that t and x are measured in units of τ_a and l, respectively, ($t \to t/\tau_a$, $x \to x/l$) and rewrite equations (1), (3) as

$$\frac{\partial a}{\partial t} = \frac{\partial^2 a}{\partial x^2} + f(a,u), \tag{4}$$

$$\epsilon \frac{{\rm d}u}{{\rm d}t} = U_0 - u - r\langle J(a,u)\rangle,$$

$$\epsilon \equiv \frac{\tau_u}{\tau_a}, \quad r \equiv RL_xL_y, \quad \langle J\rangle \equiv \frac{1}{L_x}\int_0^{L_x} J{\rm d}x. \tag{5}$$

We aim to describe *the universal features* of globally coupled dynamics of current density fronts in systems with S- and Z-shaped current-voltage characteristics and generally do not specify the dependencies $f(a,u)$ and $J(a,u)$ which underly these characteristics. In the figures we use two timely semiconductor devices – the heterostructure hot electron diode (HHED) and the double barrier resonant tunneling structure (DBRT) – as examples of S- and Z-type bistabilities, respectively. For the HHED the internal variable a has the meaning of an interface charge density; the local kinetic function $f(a,u)$ and the current density $J(a,u)$

$$f(a,u) = \frac{u-a}{(u-a)^2+1} - Ta, \quad J(a,u) = u - a \tag{6}$$

have been derived in [27]. These dependencies result in an S-shaped current-voltage characteristic as shown in Figure 1a. All variables in this model are dimensionless. We refer to [27] for physical scales and for details of the semiconductor transport model. For the DBRT the parameter a is the electron concentration in the well. The local kinetic function $f(a,u)$ and the local current density $J(a,u)$ to be used in equations (1, 3) are derived in the Appendix for the case of sequential tunneling

$$f(a,u) = \frac{1}{e}(J_{\rm ew}(a,u) - J_{\rm wc}(a)),$$

$$J(a,u) = \frac{1}{2}(J_{\rm ew}(a,u) + J_{\rm wc}(a)). \tag{7}$$

The emitter-well and the well-collector current densities $J_{\rm ew}$ and $J_{\rm wc}$, respectively, are given by equations (A.6, A.7). The corresponding Z-shaped current-voltage characteristic is shown in Figure 1b. For both models we use dimensionless variables throughout the paper.

The paper is organized as follows. In Section 2 we consider self-similar front propagation as it occurs in the voltage-controlled regime and focus on the dependence of the front velocity v upon the applied voltage u. Section 3 is devoted to the globally coupled dynamics. Here we consider the regimes corresponding to a conventional positive load resistor in the external circuit as well as the situation when the system is operated *via* an active external circuit. In Section 4 we discuss and summarize the obtained results.

2 Front velocity as a function of the applied voltage

Let us consider first the case of the voltage-driven circuit $u = {\rm const}$. In this case the front between two stationary homogneous states $J_{\rm on}(u)$ and $J_{\rm off}(u)$ propagates in a self-similar way with constant velocity v:

$$J(x,t) = J_0(x - vt),$$

$$J_0 \to J_{\rm on}, J_{\rm off} \quad \text{for} \quad x \to 0, L_x. \tag{8}$$

Here $v > 0$ holds for *hot fronts* corresponding to the propagation of the high current density state into the low current density state, and $v < 0$ holds for *cold fronts* corresponding to the propagation of the low current density state into the high current density state. Since the current density $J(x,t)$ itself does not represent an independent variable it should be expressed through the order parameter $a(x,t)$ and the applied voltage $u(t)$ according

to $J(x,t) = J\left(a(x,t), u(t)\right)$. For $u = \text{const.}$ the equivalent description in terms of a is given by

$$a(x,t) = a_0(x - vt), \quad a_0 \to a_{\rm L}, a_{\rm R} \quad \text{for} \quad x \to 0, L_x, \tag{9}$$

where the asymptotic values $a_{\rm L}$, $a_{\rm R}$ should be chosen as a_1 or a_3 according to the asymptotic values for J:

$$J_{\rm on} = J(a_{\rm L}, u), \quad J_{\rm off} = J(a_{\rm R}, u). \tag{10}$$

The front is described by equation (4) and corresponds to the propagation of a stable state into a metastable state. Relaxation of the initial profile to the asymptotic solution $a_0(x - vt)$ occurs exponentially fast [44]. It follows from equation (4) that the front width W_f is close to $W_f \approx (\partial f/\partial a)^{-1}$. We assume $W_f \ll L_x$ which justifies that the boundary conditions (8, 9) are defined on the interval $[0, L_x]$ instead of $(-\infty, +\infty)$. In the co-moving frame equation (4) takes the form

$$\frac{{\rm d}^2 a_0(x)}{{\rm d}x^2} + v\frac{{\rm d}a_0(x)}{{\rm d}x} + f(a_0, u) = 0. \tag{11}$$

Multiplying equation (11) by ${\rm d}a_0/{\rm d}x$ and integrating over $\int_0^{L_x} {\rm d}x$ we obtain the general expression for the front velocity [1]

$$v(u) = \frac{A(u)}{B(u)}, \quad A(u) \equiv \int_{a_{\rm L}}^{a_{\rm R}} f(a,u){\rm d}a,$$
$$B(u) \equiv \int_0^{L_x} ({\rm d}a_0/{\rm d}x)^2 {\rm d}x. \tag{12}$$

Since $B > 0$ the direction of the front propagation is determined by the sign of $A(u)$: we have hot fronts with $v > 0$ for $A(u) > 0$ and cold fronts with $v < 0$ for $A(u) < 0$. It can be readily seen that at the bifurcation points $u = u_{\rm h}$ and $u = u_{\rm th}$ where a new state emerges with increase or decrease of the control parameter u, respectively, the function $f(a,u)$ has a fixed sign on the whole interval $[a_1, a_3]$. The sign of $A(u)$ depends on which of the two states a_1, a_3 experiences the bifucation but is always such that the "old" state propagates into the "new" state. Therefore for S-type systems we predict hot and cold fronts for $u = u_{\rm h}$ and $u = u_{\rm th}$, respectively, whereas for Z-type systems we expect cold and hot fronts for $u = u_{\rm h}$ and $u = u_{\rm th}$, respectively. For a certain value $u_{\rm co}$ between these points $A(u_{\rm co}) = 0$ and the front has zero velocity. Assuming monotonicity, we conclude that the $v(u)$-dependencies obtained for the HHED and DBRT by direct numerical simulations (Figs. 4a and 4b) are qualitatively the same for all bistable systems with S- and Z-shaped characteristics. Note that these dependencies look similar but the direction of the front propagation is inverted.

At $u = u_{\rm h}, u_{\rm th}$ the intermediate value a_2 coincides with a_1 or a_3 and the local kinetic function is tangent to the line $f = 0$ for $a = a_2$. Our numerical simulations show that $|{\rm d}v/{\rm d}u| = \infty$ at these points (see also [39]). We propose that this is a universal feature of the $v(u)$ dependence caused by the fact that $|{\rm d}B/{\rm d}u| = \infty$ due to the divergence $|{\rm d}a_{\rm L,R}/{\rm d}u| = \infty$ at the bifurcation point.

In the $(\langle J\rangle, u)$-phase plane the trajectories corresponding to self-similar front propagation are represented by straight vertical arrows (Figs. 4c and 4d). The phase flow is directed up and down for hot and cold fronts, respectively. In a large system ($L_x \gg W_f$) the line $u = u_{\rm co}$ exactly corresponds to stationary fronts, or kinks. In a finite-size system the branch of stationary kinks slightly deviates from the vertical line in such a way that the sign of its differential conductance coincides with the differential conductivity of the intermediate branch of uniform states, *e.g.*, we have negative differential conductance (NDC) for S-shaped bistability and positive differential conductance (PDC) for Z-shaped bistability (see Figs. 4c and 4d). Let us support this observation by the following analytical arguments. The differential conductance of both homogeneous and inhomogeneous states $a_0(x)$

$$\sigma_d \equiv (L_x L_y)\frac{{\rm d}\langle J(a,u)\rangle}{{\rm d}u} = (L_x L_y)\left(\left\langle \frac{\partial J}{\partial u}\right\rangle + \left\langle \frac{\partial J}{\partial a}\frac{\delta a}{\delta u}\right\rangle\right) \tag{13}$$

can be represented as (see [26])

$$\sigma_d = \sigma_u - (L_x\ L_y)\sum_m \frac{\langle(\partial f/\partial u)\Psi_m\rangle\langle(\partial J/\partial a)\Psi_m\rangle}{\lambda_m},$$
$$\sigma_u \equiv (L_x\ L_y)\left\langle \frac{\partial J}{\partial u}\right\rangle > 0, \tag{14}$$

where σ_u denotes the differential conductance for the fixed internal parameter a, Ψ_m and λ_m are eigenmodes and eigenvalues of the corresponding stationary state, $\partial f/\partial u$ and $\partial J/\partial a$ are calculated at the stationary solution $a_0(x)$. In nonlinear systems the main contribution to the differential conductance is due to the response δa of the internal parameter upon the variation δu of the applied bias, and therefore generally $|\sigma_d| \gg \sigma_u$. The stationary front experiences a weak translation instability: this implies that only the first eigenvalue λ_1 is positive, $|\lambda_1| \ll |\lambda_m|$ for $m > 1$, and the "ground-state" eigenmode $\Psi_1 \geq 0$ corresponds to translation [22,25,26]. Therefore σ_d is determined solely by the first term in the sum in equation (14). For the homogeneous state $a_0 = a_2$ on the intermediate branch of the current-voltage characteristic the eigenmodes Ψ_m are given by $\Psi_m(x) = \cos(\pi(m-1)x/L_x)$, $\lambda_1 = \partial f/\partial a > 0$ and $\partial f/\partial u$, $\partial J/\partial a = \text{const}$. Therefore for $m > 1$ all terms in the sum in equation (14) are equal to zero. Thus, for both stationary fronts $a_0(x)$ and the homogenous states $a_0 = a_2 = \text{const.}$ we have

$$\sigma_d \approx (L_x\ L_y)\frac{\langle(\partial f/\partial u)\Psi_1\rangle\langle(\partial J/\partial a)\Psi_1\rangle}{\lambda_1},$$
$$\Psi_1 \geq 0, \quad \lambda_1 > 0 \tag{15}$$

(note that Eq. (15) is neither applicable to narrow filaments nor in the vicinity of the turning points $u = u_{\rm h}, u_{\rm th}$). According to equation (15) $\operatorname{sgn}\{\sigma_d\}$ is determined by $\operatorname{sgn}\{\partial f/\partial u\}$ and $\operatorname{sgn}\{\partial J/\partial a\}$. Assuming that the functions $\partial f/\partial u$ and $\partial J/\partial a$ are of fixed sign, which is usually the case, we conclude that $\operatorname{sgn}\{\sigma_d\}$ for stationary

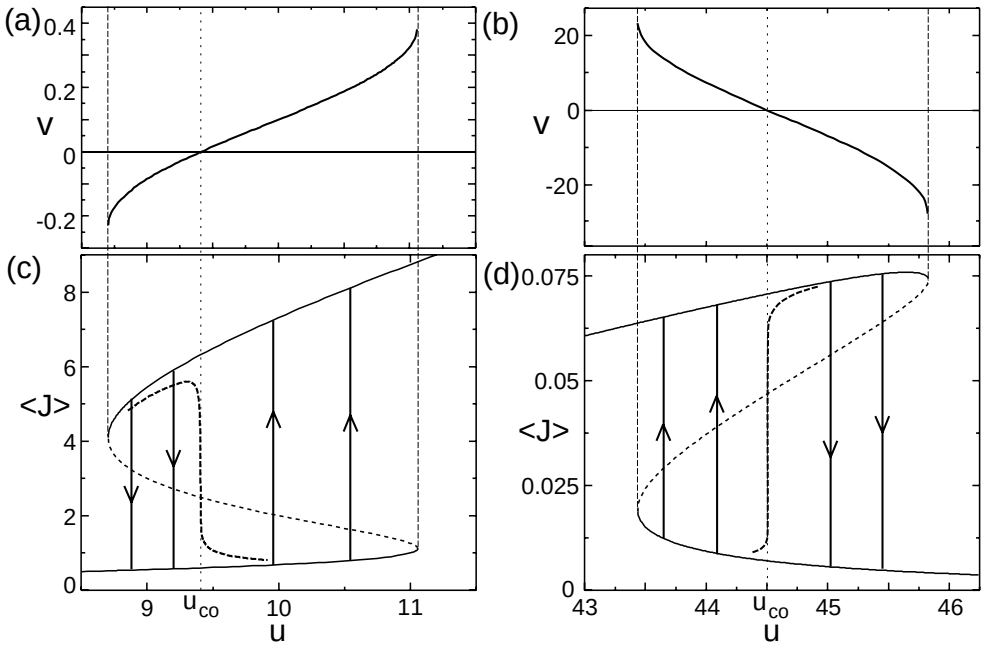

Fig. 4. Self-similar front propagation in the voltage-controlled regime u = const. for S-shaped (a, c) and Z-shaped (b, d) bistability. The front velocity v is shown in (a, b) as a function of the applied voltage u. The phase flow in the $(\langle J\rangle, u)$ plane for self-similar front propagation in the voltage-controlled regime is shown in (c, d). The thick solid line depicts the local current-voltage characteristic of uniform states. The thin solid line at $u = u_{\rm co}$ corresponds to a stationary front for $L_x \gg W_f$, the thick dashed line corresponds to the stationary fronts for finite system size $L_x \approx 5\,W_f$. The numerical parameters of the HHED ($T = 0.05$) and the DBRT (see Appendix) are used in (a, c) and (b, d), respectively.

fronts (or, more generally, for wide filaments) and for homogeneous states on the intermediate branch is the same.

The deviation of the thick dashed curve from the vertical line at $u = u_{\rm co}$ reflects the attraction of the system boundaries in a finite-size system which causes a translation instability of a stationary front ($\lambda_1 > 0$) in the voltage-controlled regime. However, this instability can hardly be detected in numerical simulations even for $L_x > 10W_f$ due to the pinning of fronts (*e.g.*, see [45]) caused in this case by the discreteness of the grid. In realistic systems of large transverse dimensions the front stability in the voltage-driven regime is determined by structural imperfections rather than by boundaries effects [26]. However, the sign of the differential conductance will be shown to have a crucial impact on the stability in presence of global coupling and will be discussed at length in the next sections.

3 Globally coupled front dynamics

3.1 Reduced equations of motion

The total current through a semiconductor element depends on the front position w, and in presence of a global constraint the control parameter u changes as the front propagates. Since the local kinetic function $f(a, u)$ and the asymptotic values $a_{\rm L}$, $a_{\rm R}$ in the globally coupled regimes are not constant, the self-similarity of front propagation is broken. Parametrizing the front by its position $w(t)$ and the values in the two phases $a_{\rm L}(t)$ and $a_{\rm R}(t)$ we can describe the front dynamics by ordinary differential equations:

$$\dot{w} = v\left\{a(x,t), u(t)\right\}, \tag{16}$$

$$\dot{a}_{\rm L}(t) = f\left(a_{\rm L}(t), u(t)\right), \tag{17}$$

$$\dot{a}_{\rm R} = f\left(a_{\rm R}(t), u(t)\right), \tag{18}$$

$$\varepsilon\dot{u} = U_0 - u - r\left[J(a_{\rm L}(t), u(t))\frac{w(t)}{L_x} + J(a_{\rm R}(t), u(t))\left(1 - \frac{w(t)}{L_x}\right)\right]. \tag{19}$$

Generally, the front velocity has a functional dependence on the instantaneous front shape and the instantaneous local kinetic profile (16) which implies that the front ansatz given by (16–18) is not complete. This difficulty can be overcome if the time hierarchy of the three following relaxation processes is properly taken into account. First, the front shape relaxes to the quasistationary shape corresponding to the local kinetic function $f(a, u)$ and instantaneous asymptotic values $a_{\rm L}$ and $a_{\rm R}$. Second, $a_{\rm L}$ and $a_{\rm R}$ relax to the quasistationary values defined by $f(a, u) = 0$. Third, the applied voltage u tends to the value $U_0 - r\langle J(t)\rangle$ given by the load line. It has been argued in [14,39] that the two first relaxation processes are fast with respect to the characteristic time W_f/v it takes for the front to advance by its own width W_f. In this case the actual velocity

v is determined by the instantaneous value of u and coincides with the velocity of self-similar propagation at this value of u. Then equations (16–19) can be considerably simplified:

$$\dot{w} = v(u), \tag{20}$$

$$\varepsilon \dot{u} = U_0 - u - r\left[J_{\rm on}(u)\frac{w(t)}{L_x} + J_{\rm off}(u)\left(1 - \frac{w(t)}{L_x}\right)\right]. \tag{21}$$

The relaxation time $\epsilon = \tau_u/\tau_a$ of the variable u is controlled by the external circuit ($\tau_u = RC$). For $C \to 0$ the feedback upon the front dynamics is instantaneous, for $C \to \infty$ the feedback vanishes and the front propagates as in the voltage-controlled case.

We have confirmed the validity of reduction (20, 21) by direct numerical simulations of the full equations (1, 3) in comparison with the predictions of the reduced model (20, 21). The deviation of the front velocity has always been found to be less than 0.5%.

3.2 Global coupling via passive external circuit (R > 0)

Qualitatively, the type of feedback on front dynamics is determined by the slope of the $v(u)$-dependence and the sign of the load resistance R in the external circuit. The propagation of hot fronts is accompanied by an increase of the total current and according to equation (3) for $R > 0$ the voltage u decreases. Taking into account that $\mathrm{d}v/\mathrm{d}u > 0$ for S-type systems and $\mathrm{d}v/\mathrm{d}u < 0$ for Z-type systems (Figs. 4a and 4b), we conclude that the front velocity decreases and increases, respectively. Similar reasoning holds for cold fronts. This results in negative feedback on front dynamics for S-type systems and positive feedback for Z-type systems.

In Figures 5 and 6, we present numerical solutions of equations (4, 5) for $R > 0$ and sufficiently small $\epsilon = \tau_u/\tau_a$. Since in this case the relaxation of u is fast, the trajectories in the $(\langle j \rangle, u)$-plane exactly follow the load lines. The front propagation is decelerated for the S-system and accelerated for the Z-system. For the load line which intersects the line $u = u_{\rm co}$ the system possesses a fixed point corresponding to a stationary front at a certain position $w = w_0$ (Figs. 5 and 6, trajectories 1, 4). This point is a stable node for the S-system (Fig. 5) and a saddle-point for the Z-system (Fig. 6). A general stability analysis of transverse current patterns has been recently performed [26]. The stability criterion is given by

$$-\sigma_u + \frac{C\lambda_1}{\tau_a} < R^{-1} < -\sigma_d, \quad C > 0, \tag{22}$$

where $\lambda_1 > 0$ is the eigenvalue of the unstable mode corresponding to translation. According to (22) only fronts with $\sigma_d < 0$ can be stabilized for $R > 0$. That implies that stationary fronts in Z-systems driven *via* an ordinary passive external circuit with $R > 0$ are never stable. The upper bound of the criterion (22) corresponds to the saddle-node bifurcation where the system has one real positive eigenvalue. That indicates that the stationary front has lost stability with respect to the translation mode, and monotonic front propagation will switch the system to the homogeneous state. The lower bound corresponds to an oscillatory instability where a pair of complex conjugate eigenvalues crosses the imaginary axis. Note that the main contribution to the differential conductivity of the stationary front comes from the shift of the front and therefore generally $|\sigma_d| \gg \sigma_u$.

With increase of $\epsilon \equiv \tau_u/\tau_a$ the system experiences a transition from instantaneous feedback to delayed feedback. Now the slow relaxation of u results in deviations of the trajectories from the load line. For S-shaped characteristics the fixed point evolves from a stable node to a stable focus (Fig. 7). This corresponds to oscillatory transient processes leading to the steady state (Fig. 7, trajectories 1, 4). For sufficiently slow feedback the front propagation becomes self-similar as in the case of the voltage-controlled conditions. For the stationary pattern the increase of ϵ eventually leads to a violation of the left inequality in (22) and the fixed point becomes an unstable focus reflecting an oscillatory instability of the stationary front (see [39] for an example of such behaviour). However, since this instability is caused by the interaction of the front wall with the boundaries it represents essentially *a boundary effect* which is not relevant for the front dynamics in a large system ($W_f \ll L_x$). For Z-systems the phase portrait does not undergo qualitative changes with increase of ϵ and the stationary point always remains a saddle-point.

3.3 Global coupling via active external circuit (R < 0)

The type of feedback can be changed if the system is operated by an active circuit simulating a negative load resistance $R < 0$. Such a circuit has been implemented in [46] in order to stabilize the uniform states corresponding to the intermediate branch of the DBRT current-voltage characteristic and can also be used in studies of lateral patterns. Note that to secure $\tau_u = RC > 0$ such a circuit should also provide $C < 0$.

For $R < 0$ the propagation of a hot front is accompanied by an increase of u. That results in positive feedback for S-systems and negative feedback for Z-systems. The last case is most interesting here since efficient control over front propagation and stabilization of lateral patterns becomes possible. The front dynamics in a Z-system for $R < 0$ and instantaneous feedback is illustrated in Figure 8. Now the front propagation in the Z-system is decelerated. For $C < 0$ the stability criterion takes the form [26]

$$-\sigma_d < R^{-1} < -\sigma_u + \frac{C\lambda_1}{\tau_a}, \quad C < 0. \tag{23}$$

In equation (23) the lower and upper bounds correspond to a saddle-node bifurcation and oscillatory instabilities, respectively. According to (23) a stationary pattern with

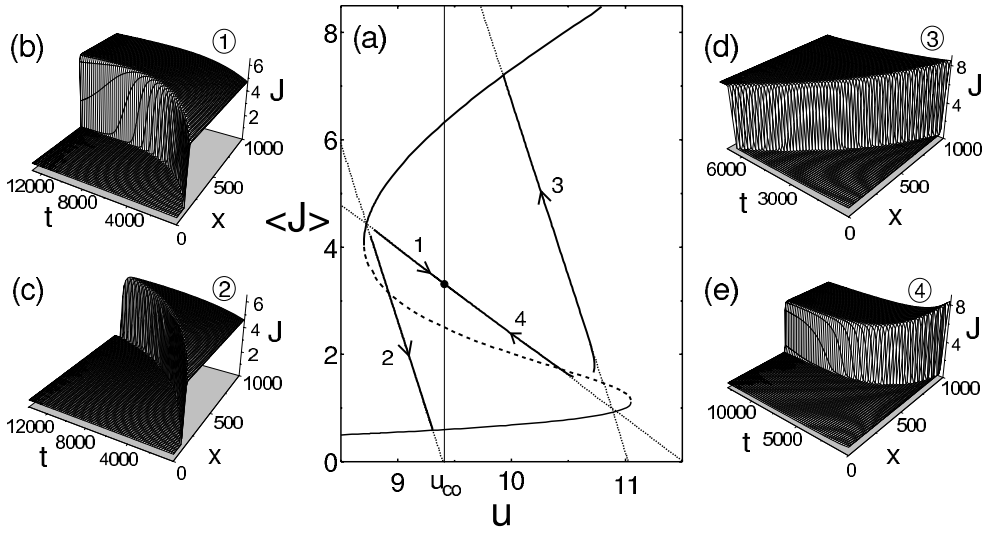

Fig. 5. Globally coupled dynamics of lateral current density fronts in an S-system (HHED) for positive load $R > 0$ and instantaneous feedback. (a) Phase portrait including the S-shaped current-voltage characteristic (solid line) with different load lines (dotted). The front dynamics is indicated by the trajectories 1, 2, 3, 4. The fixed point at $u = u_{\rm co}$ is a stable node, and corresponds to a stationary front. (b, c) Decelerated cold fronts evolving either to a stationary front (b; trajectory 1) or to the uniform off-state (c; trajectory 2). (d, e) Decelerated hot fronts evolving either and to a stationary front (e; trajectory 4), or to the uniform on-state (d; trajectory 3). Parameters of the load lines: $U_0 = 11.5$, $r = 0.42$ for trajectories 1 and 4, $U_0 = 9.4$, $r = 0.15$ for trajectory 2 and $U_0 = 11.0$, $r = 0.15$ for trajectory 3; $\epsilon = 100$, $L_x = 1000$.

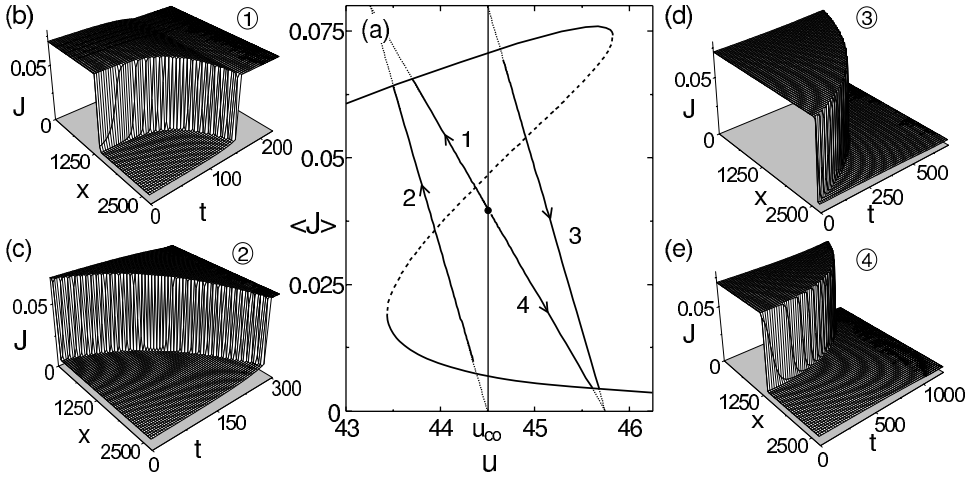

Fig. 6. Globally coupled dynamics of lateral fronts in a Z-system (DBRT) for positive load $R > 0$ and instantaneous feedback. (a) Phase portrait including the Z-shaped current-voltage characteristic (solid line) with different load lines (dotted). The front dynamics is indicated by the trajectories 1, 2, 3, 4. The fixed point at $u = u_{\rm co}$ is a saddle-point. The regimes corresponding to the trajectories 1 and 4 can be realized only for special initial conditions. (b, c) Accelerated hot fronts for trajectories 1 (b) and 2 (c). (d, e) Accelerated cold fronts for trajectories 3 (d) and 4 (e). Parameters of the load lines: $U_0 = 45.75$, $r = 31.25$ for trajectories 1 and 4; $U_0 = 44.5$, $r = 15.62$ for trajectory 2, $U_0 = 45.75$, $r = 15.62$ for trajectory 3; $\epsilon = 10^{-12}$, $L_x = 2750$.

$\sigma_d > 0$ can be stable for $R < 0, C < 0$. For sufficiently small C the fixed point is a stable node as in Figure 8. Increase of $\epsilon = \tau_u/\tau_a$ leads to oscillatory motion as shown in Figure 9, the fixed point becomes a stable focus. It is readily seen that the front behavior in Z-type systems for $R < 0$ is qualitatively the same as in S-type systems for $R > 0$.

However, the implementation of the active external circuit leads also to some new regimes which have no analogue for $R > 0$. First of all, if a spatially extended bistable element is operated *via* an active external circuit temporal instabilities can be caused by the negative differential conductivity of this circuit itself. Indeed, for $R^{-1} > -\sigma_u$ the condition for an oscillatory instability is fulfilled even for $C = O$. This instability is not related to front oscillations but represents circuit induced oscillations. These oscillations can be excluded by choosing a negative relaxation time in the external circuit.

For $R^{-1} > \sigma_u$, $\tau_u < 0$, $R < 0$, $C > 0$ we can also meet a new situation if the slope of the load line is smaller than

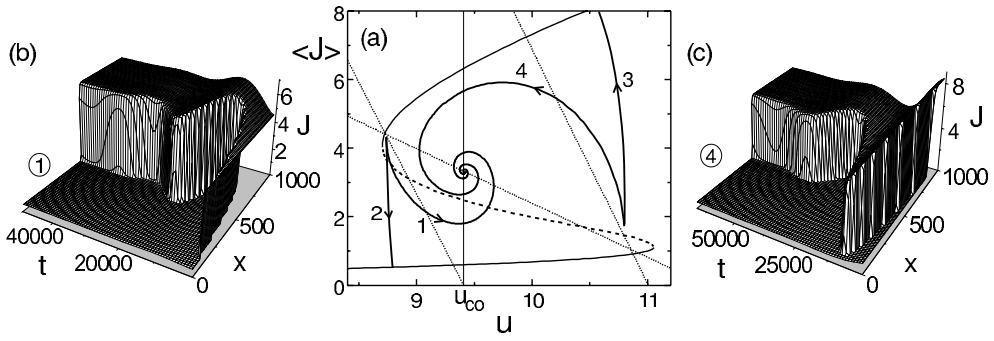

Fig. 7. Oscillatory dynamics of globally coupled fronts in an S-system (HHED) in the case of delayed feedback ($R > 0$). (a) Phase portrait including the S-shaped current-voltage characteristic (solid line). The load lines (dotted) and the initial conditions are as in Figure 5, $\epsilon = 10^4$. In contrast to Figure 5 the trajectories 1, 2, 3, 4 deviate from the corresponding load lines due to the delay in the feedback. The fixed point at $u = u_{\rm co}$ is a stable focus. (b, c) Oscillatory slowing down of the cold (b) and hot (c) front corresponding to trajectories 1 and 4, respectively.

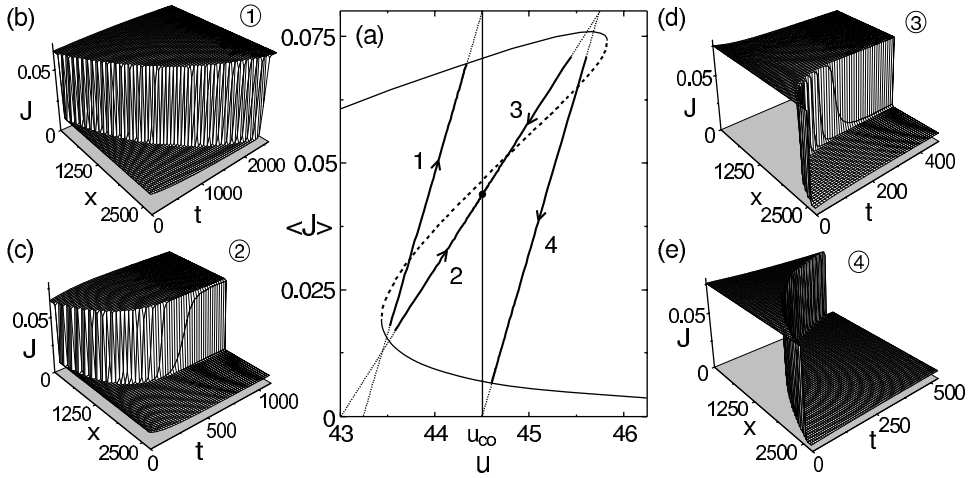

Fig. 8. Globally coupled dynamics of lateral fronts in a Z-system (DBRT) operated *via* an active external circuit with $r < 0$, $\epsilon > 0$ ($R < 0$, $C < 0$). The relaxation time $\epsilon = 10^{-12}$ corresponds to instantaneous feedback. (a) Phase portrait including the Z-shaped current-voltage characteristic (solid line) and load lines (dotted). The fixed point at $u = u_{\rm co}$ is a stable node. (b, c) Decelerated hot fronts evolving either to the uniform on-state (b; trajectory 1) or to a stationary front state (c; trajectory 2). (d, e) Decelerated cold fronts evolving either to a stationary front state (d; trajectory 3) or to the uniform off-state (e; trajectory 4). Parameters of the load lines: $U_0 = 43.25$, $r = -15.62$ for trajectory 1; $U_0 = 43$, $r = -34.37$ for trajectories 2, 3; $U_0 = 44.5$, $r = -15.62$ for trajectory 4.

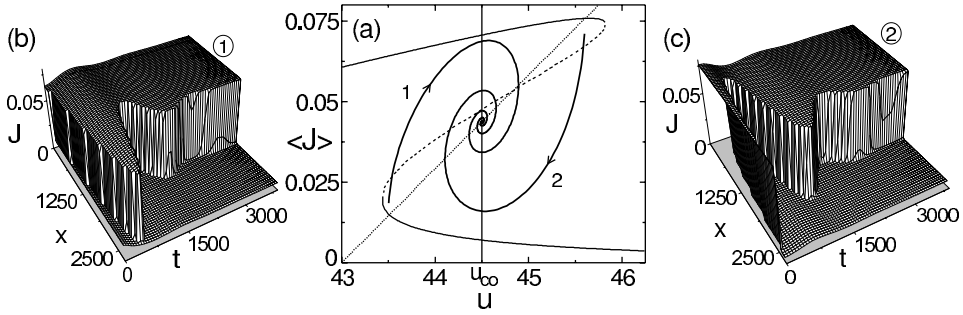

Fig. 9. Oscillatory dynamics of current density fronts in a Z-system (DBRT) for $R < 0, C < 0$ in the case of delayed feedback $\epsilon = 10^{-9}$. (a) Phase portrait including the Z-shaped current-voltage characteristic (solid line). The load line (dotted) corresponds to $U_0 = 43$, $r = -34.37$. (b, c) Oscillatory slowing down of the cold (b) and hot (c) front corresponding to the trajectories 1 and 2, respectively.

the slope of the on- and off-branches of the current-voltage characteristic. Generally, these regimes are of limited interest since: (i) being close to the current-controlled condition they are not favorable for front propagation since the load line does not connect on- and off-branches of the current-voltage characteristic within the bistability regime; (ii) the global dynamics becomes unbounded in this case as an effect of the active circuit. Let us note that for $R^{-1} > \sigma_u$ the propagation of a hot or cold front can be accompanied by a decrease or increase, respectively, of $\langle J \rangle$. Indeed, eliminating u adiabatically from (20, 21), by direct calculation we obtain:

$$\frac{\mathrm{d}J}{\mathrm{d}t} = \frac{1}{L_x} \frac{J_{\mathrm{on}}(u) - J_{\mathrm{off}}(u)}{1 + R\sigma_u} v(t). \tag{24}$$

Therefore if $(1 + R\sigma_u) < 0$ we have $\mathrm{d}J/\mathrm{d}t < 0$ for $v > 0$. This regime, where the type of feedback may become *indeterminate*, has been studied in [39] for the model of a gate-driven *p*-*n*-*p*-*n*-structure.

4 Discussion and conclusion

In this article we have studied the dynamics of lateral current density fronts in bistable semiconductor systems with S- and Z-shaped current-voltage characteristics (Figs. 1 and 2). Both hot fronts ($v > 0$, high current state propagates into low current state) and cold fronts ($v < 0$, low current state propagates into high current state) can be excited in these systems for $u_{\mathrm{h}} < u < u_{\mathrm{th}}$. In the voltage controlled case the front propagates in a self-similar way and the direction as well as the absolute value of the velocity can be controlled by varying u (Figs. 4a and 4b). The front has zero velocity for a certain voltage u_{co} determined by the equal areas rule $A = 0$ (see Eq. (12)). The direction of the front propagation is different for S- and Z-type systems, which is reflected by the different sign of the slopes of the $v(u)$-dependence.

In the presence of global coupling *via* an external circuit the voltage u applied to the structure varies as the front propagates due to the dependence of the total current on the front position. This results in a feedback upon the front dynamics. The type of this feedback is determined by the slope of the $v(u)$-dependence and the type of external load. For positive external load $R > 0$ the feedback is negative for S-systems and positive for Z-systems (Figs. 5 and 6). This results in deceleration and acceleration of the front propagation, respectively. The type of the feedback can be reversed if the system is operated *via* an active external circuit simulating negative load $R < 0$ and capacitance $C < 0$ (the latter is required in order to keep the relaxation time RC positive). The case of negative feedback (for Z-systems) is of most interest since deceleration and efficient control over fronts in Z-systems becomes possible (Fig. 8). The propagation of globally coupled fronts is monotonic as long as the relaxation time of the external circuit $\tau_u = RC$ is sufficiently small and the feedback upon the front dynamics is instantaneous (Figs. 5 and 6). Delayed negative feedback can result in oscillatory slowing down in both S- and Z-systems as shown in Figure 7 and Figure 9, respectively. Generally, we conclude that S- and Z-systems are dual and the behaviour of S-type systems for $R > 0$ or $R < 0$ is qualitatively the same as the behaviour of Z-type systems for $R < 0$ or $R > 0$, respectively. The heterostructure hot electron diode (S-system) and the double-barrier resonant tunneling structure (Z-system) which we have used to illustrate our findings serve as prominent examples of semiconductor heterostructures falling into these two classes.

Despite of the fact that globally coupled front propagation is not self-similar, due to the fast relaxation of the front profile the front velocity is determined by the instantaneous value of the voltage u with good accuracy. Therefore the equations of motion can be reduced to (20, 21).

The type of the feedback upon propagating fronts is closely related to the stability of stationary lateral patterns considered in [25,26]. It is known that in the presence of global coupling the stability of an inhomogeneous pattern (stationary lateral current density front or filament) which has one unstable mode in the voltage controlled regime is determined by the sign of its differential conductance. Figure 4c and 4d helps to understand the stability criterion qualitatively. In the globally coupled regime the stability of the steady state is determined by the projection of the phase flow onto the load line. For $\sigma_d < 0$ this projection is directed towards the steady point for $R > 0$, indicating stability, as it happens in S-systems, for $\sigma_d > 0$ this holds for $R < 0$, as it happens in Z-systems.

Operating the system *via* an active external circuit with $R < 0$ results in new effects which do not exist for conventional circuits. If a spatially extended nonlinear element is operated with a load $R < 0$, a temporal instability can be induced by the active circuit itself. Therefore such circuits should provide $C < 0$ in order to exclude circuit-induced relaxation-type oscillations in the regimes considered above.

Globally coupled dynamics of travelling pulses in *excitable media* has recently been studied in [18]. Global coupling influences the velocity of a travelling pulse but the self-similar character of the motion remains. As it has been shown here in *bistable media* the global coupling completely destroys the self-similarity, resulting in accelerated, decelerated or oscillatory motion. These findings have important consequences for gate-driven bistable systems where the front dynamics experiences a feedback from both the gate and the main external circuits. Generally, these systems should be considered as bistable media with two global constraints [43]. Recently it has been shown that gate-driven *p*-*n*-*p*-*n*-structures possess an Z-shaped and an S-shaped current-voltage characteristics in the gate (cathode-gate) and the main (cathode-anode) circuits, respectively. The interplay between the positive feedback *via* the gate circuit (*activatory global constraint*) and negative feedback *via* the main circuit may result in *large-amplitude self-sustained oscillations* of the front [47].

It is important to note that in semiconductor switching devices with S-shaped current-voltage characteristics (*e.g.*, in thyristors) turn-on and -off can often be triggered locally *via* the propagation of current density fronts [42].

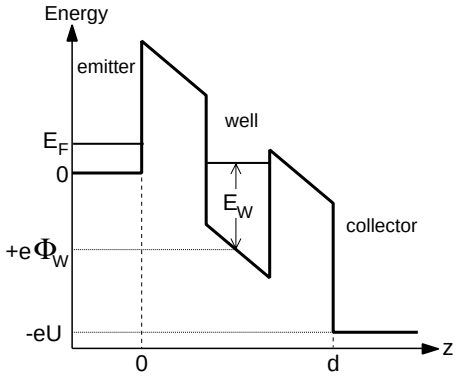

Fig. 10. Schematic potential profile of the double barrier resonant tunneling structure.

Since the device operation implies not only switching from a low current state to a high current state but also from a high voltage state to a low voltage state, the semiconductor device essentially interacts with the external circuit during this transient process and the propagation of the current density front experiences a strong global coupling. It is not sufficient to treat only self-similar propagating fronts in this case. Additionally, nonuniform attractors (stationary filamentary states) of the transient process should be properly taken into account [34]. The concepts of globally coupled front dynamics which we have developed here provide an adequate description of inhomogenous switching processes in these devices.

Appendix A: Model for the double-barrier resonant tunneling diode

The intrinsic bistability of the double-barrier resonant tunneling diode (DBRT) occurs due to the dynamical charge accumulation within the potential well. The built-up charge leads to an electrostatic feedback mechanism which increases the energy of the quasi-bound state supporting resonant tunneling conditions for higher applied voltages. This may result in bistability and hysteresis where a high current and a low current state coexist for the same applied voltage u and the current voltage characteristic becomes Z-shaped rather than the conventional N-shaped characteristic associated in general with resonant tunneling [38]. Recently it has been pointed out [40,41] that such bistability provides a basis for lateral pattern formation in the DBRT. In this Appendix we derive a nonlinear reaction-diffusion model for the DBRT in the bistable regime which is used as an example of a system with Z-shaped current-voltage characteristic in our simulations of globally coupled front dynamics.

We consider a symmetric resonant tunnelling structure and assume incoherent sequential tunneling for the vertical (along z-axis) transport (Fig. 10). We characterize the internal state of the device by the built-up electron concentration $n(x, y, t)$ in the well. The continuity equation for $n(x, y, t)$ has the form

$$\frac{\partial n}{\partial t} + \frac{1}{e}\nabla_\perp \mathbf{J}_\perp = \frac{1}{e}\left(J_{\rm ew}(n, U) - J_{\rm wc}(n)\right), \qquad \nabla_\perp \equiv \mathbf{e}_x\frac{\partial}{\partial x} + \mathbf{e}_y\frac{\partial}{\partial y}, \tag{A.1}$$

where $e < 0$ is the electron charge, U is the applied voltage, $J_{\rm ew}(x, y)$ and $J_{\rm wc}(x, y)$ are the local densities of the emitter-well and the well-collector currents, respectively, $\mathbf{J}_\perp$ is the density of the transverse current in the well.

The emitter-well current density $J_{\rm ew}$ can be evaluated up to lowest order in the coupling in the spirit of [48]. Assuming conservation of the transverse momentum $\mathbf{k}$ during the tunneling process and neglecting the broadening of the states in the emitter we obtain

$$J_{\rm ew} = \frac{2e}{L_x L_y}\sum_{\mathbf{k}}\sum_{q}\frac{2\pi}{\hbar}|H_q^2|\Theta(E_{\rm F} - E_k - E_q)\frac{1}{2\pi} \times A_{\rm w}(E_q + E_k - E_{\rm w} - e\phi_{\rm w}, \mathbf{k})(1 - f_{\rm w}), \tag{A.2}$$

where q and $\mathbf{k}$ are vertical and transverse wave vectors of the electrons in the emitter, respectively. $E_q = \hbar^2 q^2/2m$ and $E_k = \hbar^2\mathbf{k}^2/2m$ are the corresponding kinetic energies (here m is the effective electron mass) and H_q is the matrix element of the emitter-well transition. $\Theta(E)$ is the step function describing the occupation of the emitter up to the Fermi energy $E_{\rm F}$ for zero temperature. $A_{\rm w}(E, \mathbf{k})$ is the spectral function of the bound state in the well (binding energy $E_{\rm w}$), which has still the transverse degree of freedom $\mathbf{k}$. $\phi_{\rm w}$ is the electrical potential at the bottom of the well (the potential of the emitter is taken to be zero). Finally $f_{\rm w}$ is the filling factor for the states in the well, which we estimate by a homogeneous distribution of the electron density up to the Fermi energy

$$f_{\rm w}(n) = \frac{n}{\rho_0(E_{\rm F} - E_{\rm w} - e\phi_{\rm w})}, \tag{A.3}$$

where $\rho_0 \equiv m/\pi\hbar^2$ is the two-dimensional density of states. In the following we assume $A_{\rm w}(E, \mathbf{k}) = \Gamma/[(E - E_k)^2 + \Gamma^2/4]$, where $\Gamma \equiv \Gamma_{\rm L} + \Gamma_{\rm R} + \Gamma_{\rm scatt} = $ const. is the total broadening of the quasibound well state resulting from the escape *via* emitter-well barrier, well-collector barrier and scattering in the well, respectively. Then we obtain in the continuum limit ($\sum_{\mathbf{k}}\sum_q \to L_x L_y L_z/(2\pi)^3 \int {\rm d}^2k \int {\rm d}q$):

$$J_{\rm ew} = \frac{e}{2\pi\hbar}\rho_0\int_0^{E_{\rm F}} {\rm d}E_q (E_{\rm F} - E_q)\frac{2m|H_q^2|L_z}{\hbar^2 q} \times \frac{\Gamma}{(E_q - E_{\rm w} - e\phi_{\rm w})^2 + \Gamma^2/4}(1 - f_{\rm w}). \tag{A.4}$$

In the following $\Gamma_{\rm L} \equiv 2m|H_q^2|L_z/(\hbar^2 q)$ is taken to be constant for simplicity.

For $n = 0$ the energy of the bottom of the well in a symmetric structure is given by $\phi_{\rm w} = -U/2$. Due to the built-up charge $\phi_{\rm w}$ depends also on the electron concentration $n(x, y)$ in the well. Assuming that transverse variations

of $n(x,y)$ are smooth in a sense that their characterstic wavelength is much larger than the effective thickness of the structure d, we can represent the corresponding correction locally as $\Delta\phi_{\rm w}(n) = en/C_{\rm int}$, where $C_{\rm int}$ is an effective capacitance per area of the well. This yields (see [40,41])

$$\phi_{\rm w} = -\frac{U}{2} + \frac{en}{C_{\rm int}}, \quad C_{\rm int} = \frac{2\epsilon\epsilon_0}{d}, \tag{A.5}$$

where ϵ and ϵ_0 denote the relative and absolute permittivity, respectively.

With these ingredients the evaluation of equation (A.4) gives the final formula

$$J_{\rm ew}(n,U) = \frac{e}{\hbar}\Gamma_{\rm L}\rho_0\left[\Delta(n,U)\frac{\arctan(2\Delta/\Gamma)-\arctan(2\Omega/\Gamma)}{\pi} - \frac{\Gamma}{4\pi}\ln\left(\frac{\Delta^2+(\Gamma/2)^2}{\Omega^2+(\Gamma/2)^2}\right)\right](1-\frac{n}{\rho_0\Delta}), \tag{A.6}$$

$$\Delta(n,U) \equiv E_{\rm F} - E_{\rm w} + \frac{eU}{2} - \frac{e^2 n}{C_{\rm int}},$$
$$\Omega(n,u) \equiv \frac{eU}{2} - \frac{e^2 n}{C_{\rm int}} - E_{\rm w},$$

where Δ and Ω denote the energy of the quasibound state with respect to the Fermi level and bottom of the conductance band in the emitter, respectively. Since the bottom of the conductance band of the collector is much lower than the quasibound state (Fig. 10) if a negative bias U is applied, the well-collector current can be taken as proportional to n

$$J_{\rm wc} = \frac{e}{\hbar}\Gamma_{\rm R} n, \tag{A.7}$$

where $\Gamma_{\rm R}/\hbar$ is the escape rate *via* the well-collector barrier.

The transverse current in the well is described in the drift-diffusion approximation:

$$\mathbf{J}_\perp = |e| n\mu \mathbf{F}_\perp - eD_0\nabla_\perp n, \tag{A.8}$$

where μ and D_0 are the mobility and the diffusion coefficient in the well, respectively. $\mathbf{F}_\perp = -\nabla_\perp\phi_{\rm w}$ is the transverse electrical field in the well. Taking into account (A.5), we conclude that the transverse coupling in the DBRT is effectively due to a concentration-dependent diffusion term

$$\mathbf{J}_\perp = -eD(n)\nabla_\perp n, \quad D(n) \equiv D_0 + \frac{|e|\mu n}{C_{\rm int}}\cdot \tag{A.9}$$

Substituting (A.9) into (A.1) we arrive at the following reaction-diffusion equation which describes the internal dynamics in the DBRT:

$$\frac{\partial n}{\partial t} = \frac{1}{e}\left[J_{\rm ew}(n,u) - J_{\rm wc}(n)\right] + \nabla_\perp\left[D(n)\nabla_\perp n\right]. \tag{A.10}$$

In the following we simplify the consideration assuming an effective diffusion coefficient $D = \text{const}$. The current densities $J_{\rm ew}$ and $J_{\rm wc}$ are given by (A.6, A.7), respectively.

The dynamical equation for U has been derived in the general form in [29] from Kirchhoff's and Ampere's law with proper account taken for the displacement currents within the semiconductor element:

$$RC\frac{{\rm d}U}{{\rm d}t} = U_0 - U - R\frac{\widetilde{C}}{L_x L_y}\int_0^{L_x}\int_0^{L_y}\int_0^d {\rm d}x\,{\rm d}y\,{\rm d}z\frac{J_z(z)}{\epsilon(z)},$$
$$\frac{1}{\widetilde{C}} = \int_0^d \frac{{\rm d}z}{L_x L_y \epsilon(z)}, \tag{A.11}$$

where $J_z(z)$ is the vertical component of the current density, $\epsilon(z)$ is the device permittivity and $\widetilde{C}$ is an effective intrinsic sample capacitance. For the symmetric DBRT considered here, we have $J_z(z) = J_{\rm ew}$ for $0 < z < d/2$, $J_z(z) = J_{\rm wc}$ for $d/2 < z < d$, and therefore we find

$$RC\frac{{\rm d}U}{{\rm d}t} = U_0 - U - R\int_0^{L_x}\int_0^{L_y}{\rm d}x\,{\rm d}y\frac{J_{\rm ew}(n,U)+J_{\rm wc}(n)}{2}\cdot \tag{A.12}$$

We use the following structural parameters: $E_{\rm F} = 5$ meV, $E_{\rm w} = 40$ meV, $d = 20$ nm, $\Gamma_{\rm scatt} = 1$ meV, $\Gamma_{\rm L} = \Gamma_{\rm R} = 0.5$ meV, $\epsilon = 12$, $m = 0.067$ (for GaAs), and transform to dimensionless variables according to $a = n/(\rho_0 E_{\rm F})$, $u = eU/\Gamma$, $\tilde{J} = \hbar J/(e\rho_0 E_{\rm F}\Gamma)$, $\tilde{t} = t/\tau_a$ and $\tilde{x} = x/\sqrt{D\tau_a}$ (and subsequently omit the tilda). Choosing $\tau_a = \hbar/\Gamma$, from (A.10, A.12) we obtain the dimensionless equations (4, 5) with

$$f(a,u) = \tilde{J}_{\rm ew}(a,u) - \tilde{J}_{\rm wc}(a), \tag{A.13}$$

$$J(a,u) = \frac{\tilde{J}_{\rm ew}(a,u)+\tilde{J}_{\rm wc}(a)}{2}, \tag{A.14}$$

$$r \equiv RL_x L_y e^2\rho_0 E_{\rm F}/\hbar. \tag{A.15}$$

Consequently, in the DBRT model the units of time, voltage and current density are $\tau_a \approx 3.3$ ps, $\Gamma/e = 2$ mV and $(e\rho_0 E_{\rm F}\Gamma)/\hbar \approx 70.2$ kA/cm^2, respectively. The length scale $l = \sqrt{(D\tau_a)}$ scales with the square root of the effective transverse diffusion constant D; $D = 100$ cm^2/s, for instance, yields $l \approx 180$ nm. The stationary current-voltage characteristic $J = J_{\rm ew} = J_{\rm wc}$ which results from (A.10, A.6, A.7) is shown in Figure 1b.

References

1. A.S. Mikhailov, *Foundation of Synergetics* (Springer, Berlin, 1994), Vol. 1.
2. Y.B. Zeldovich, D.A. Frank-Kamenetzki, Acta Physicochimica URSS **9**, 100 (1938), also in [6], p. 131.
3. J.B. Gunn, IBM J. Res. Dev. **8**, 141 (1964).
4. L.B. Loeb, Science **148**, 1417 (1965).
5. V.L. Bonch-Bruevich, I.P. Zvyagin, A.G. Mironov, *Domain Electrical Instabilities in Semiconductors* (Consultant Bureau, New York, 1975).

6. *Dynamics of Curved Fronts*, edited by P. Pelcé (Academic Press, Boston, 1988).
7. M.P. Shaw, V.V. Mitin, E. Schöll, H.L. Grubin, *The Physics of Instabilities in Solid State Electron Devices* (Plenum Press, New York, 1992).
8. Y. Kuramoto, *Chemical Oscillations, Waves and Turbulence* (Springer-Verlag, 1988).
9. A. Kolmogorov, I. Petrovsky, N. Piskunov, Bull. Mosc. St. Univ. Ser. A **1**, 1 (1937), also in [6], p. 105.
10. Yu.M. Svirezhev, *Nonlinear Waves, Dissipative Structures and Catastrophies in Ecology* (Nauka, Moscow, 1987) (*in Russian*).
11. M. Falcke, H. Engel, M. Neufeld, Phys. Rev. E **52**, 763 (1995).
12. D. Battogtokh, A.S. Mikhailov, Physica D **90**, 84 (1996).
13. A. Pikovsky, M. Rosenblum, J. Kurths, Europhys. Lett. **34**, 165 (1996).
14. F.J. Elmer, Phys. Rev. A **41**, 4174 (1990); Z. Phys. B **87**, 377 (1992).
15. L. Schimansky-Geier, Ch. Zülicke, E. Schöll, Z. Phys. B **84**, 433 (1991); Physica A **188**, 436 (1992).
16. I. Schebesch, H. Engel, *Self-Organization in Activator-Inhibitor Systems: Semiconductors, Gas Discharge, and Chemical Active Media*, edited by H. Engel, F.-J. Niedernostheide, H.G. Purwins, E. Schöll (Wissenschaft & Technik, Berlin, 1996), p. 120.
17. F.-J. Niedernostheide, M. Or-Guil, M. Kleinkes, H.-G. Purwins, Phys. Rev. E **55**, 4107 (1997).
18. H. Hempel, I. Schebesch, L. Schimansky-Geier, Eur. Phys. J. B **2**, 399 (1998).
19. M. Falcke, H. Engel, Phys. Rev. E. **50**, 1353 (1994).
20. M. Bär, M. Falcke, M. Hildebrand, M. Neufeld, H. Engel, M. Eiswirth, Int. J. Bifur. Chaos **4**, 499 (1994).
21. N. Mazouz, G. Flätgen, K. Krischer, Phys. Rev. E **55**, 2260 (1997).
22. E. Schöll, *Nonequilibrium Phase Transitions in Semiconductors* (Springer, Berlin, 1987).
23. B.S. Kerner, V.V. Osipov, *Autosolitons* (Kluwer Academic Publishers, Dordrecht, 1994).
24. A.F. Volkov, Sh.M. Kogan, Usp. Phys. Nauk **96**, 633 (1968) [Sov. Phys. Usp. **11**, 881 (1969)].
25. F.G. Bass, V.S. Bochkov, Yu. Gurevich, Th. Eksp. Teor. Phys. **58**, 1814 (1970) [Sov. Phys. JETP **31**, 972 (1970)].
26. A. Alekseev, S. Bose, P. Rodin, E. Schöll, Phys. Rev. E **57**, 2640 (1998).
27. A. Wacker, E. Schöll, Z. Phys. B. **93**, 431 (1994).
28. F.-J. Niedernostheide, H.-J. Schulze, S. Bose, A. Wacker, E. Schöll, Phys. Rev. E **54**, 1253 (1996).
29. A. Wacker, E. Schöll, J. Appl. Phys. **78**, 7352 (1995).
30. D. Jäger, H. Baumann, R. Symanczyk, Phys. Lett. A **117**, 141 (1986).
31. V.V. Osipov, V.A. Kholodnov, Mikroelectrnoika **2**, 529 (1973) (*in Russian*).
32. K. Hess, T.K. Higman, M.A. Emanuel, J.J. Coleman, J. Appl. Phys. **60**, 3775 (1986).
33. A.M. Belyantsev, A.A. Ignatov, V.I. Piskarev, M.A. Sinitsyn, V.I. Shashkin, B.S. Yavich, M.L. Yakovlev, JETP Lett. **43**, 437 (1986).
34. A. Gorbatyuk, P. Rodin, Solid-State Electron. **35**, 1359 (1992).
35. F.-J. Niedernostheide, M. Ardes, M. Or-Guil, H.-G. Purwins, Phys. Rev. B. **49**, 7370 (1994).
36. A. Gorbatyuk, F.-J. Niedernostheide, Physica D **99**, 339 (1996).
37. S.M. Sze, *Modern Semiconductor Device Physics* (Willey, New York, 1998).
38. V.J. Goldmann, D.C. Tsui, J.E. Cunningham, Phys. Rev. Lett. **58**, 1256 (1987).
39. M. Meixner, P. Rodin, E. Schöll, Phys. Rev. E **58**, 2796 (1998).
40. B. Glavin, V. Kochelap, V. Mitin, Phys. Rev. B **56** 13346 (1997).
41. D. Mel'nikov, A. Podlivaev, Semiconductors **32**, 206 (1998).
42. M. D'yakonov, M. Levinstein, Fiz. Tekn. Poluprovodn. **12**, 729 (1978) [Sov. Phys. Semicond. **12**, 426 (1978)].
43. A. Gorbatyuk, P. Rodin, Z. Phys. B **104**, 45 (1997).
44. U. Ebert, W. van Saarlos, Phys. Rev. Lett. **80**, 1650 (1998).
45. I. Mitkov, K. Kladko, J. Peanson, Phys. Rev. Lett. **81**, 5453 (1998).
46. A. Martin, M. Lerch, P. Simmonds, L. Eaves, Appl. Phys. Lett. **64**, 1248 (1994).
47. M. Meixner, P. Rodin, E. Schöll, Phys. Rev. E **58**, 5586 (1998).
48. G.D. Mahan, *Many-Particle Physics* (Plenum, New York, 1990), Sect. 9.3.